Preparation and characterization of TiO_2 photocatalysts by Fe^{3+} doping together with Au deposition for the degradation of organic pollutants

Yongmei Wu, Jinlong Zhang *, Ling Xiao, Feng Chen

Lab for Advanced Materials and Institute of Fine Chemicals, East China University of Science and Technology, 130 Meilong Road, Shanghai 200237, PR China

A B S T R A C T

Fe^{3+} doped TiO_2 deposited with Au (Au/Fe–TiO_2) was successfully prepared with an attempt to extend light absorption of TiO_2 into the visible region and reduce the rapid recombination of electrons and holes. The samples were characterized by X-ray diffraction (XRD), N_2 physical adsorption, Raman spectroscopy, atomic absorption flame emission spectroscopy (AAS), UV–vis diffuse reflectance spectroscopy, X-ray photoelectron spectroscopy (XPS), and photoluminescence (PL) spectra. The photocatalytic activities of the samples were evaluated for the degradation of 2,4-chlorophenol in aqueous solutions under visible light ($\lambda > 420$ nm) and UV light irradiation. The results of XRD, XPS and high-resolution transmission electron microscopy (HRTEM) analysis indicated that Fe^{3+} substituted for Ti^{4+} in the lattice of TiO_2, Au existed as Au^0 on the surface of the photocatalyst and the mean particle size of Au was 8 nm. Diffuse reflectance measurements showed an extension of light absorption into the visible region for Au/Fe–TiO_2, and PL analysis indicated that the electron–hole recombination rate has been effectively inhibited when Au deposited on the surface of Fe-doped TiO_2. Compared with Fe doped TiO_2 sample and Au deposited TiO_2 sample, the Au/Fe–TiO_2 photocatalyst exhibited excellent visible light and UV light activity and the synergistic effects of Fe^{3+} and Au was responsible for improving the photocatalytic activity.

© 2008 Elsevier B.V. All rights reserved.

1. Introduction

Nanosized TiO_2 as one of the most promising photocatalysts has long been investigated for photocatalytic degradation of organic pollutants, photocatalytic dissociation of water, solar energy conversion and disinfection [1–5]. However, because of its large band gap of 3.2 eV, TiO_2 can only be excited by a small UV fraction of solar light, which has practically ruled out the use of sunlight as an energy source. Secondly, the high rate of electron–hole recombination often results in a low quantum yield and poor efficiency of photocatalytic reactions. These fundamental problems prevent TiO_2 from practical application.

In recent years, great efforts have been made to develop TiO_2-based photocatalysts sensitive to visible light in order to make use of solar energy more efficiently in practical applications [6–10]. Metal-doped TiO_2 has been widely studied for improving photocatalytic performance on the degradation of various organic pollutants under visible light irradiation [11–18]. Choi et al. conducted a systematic study on the photocatalytic activity of TiO_2 nanoparticles doped with 21 transition metal elements and found that doping with Fe^{3+}, Mo^{5+}, Ru^{3+}, Os^{3+}, Re^{5+}, V^{4+}, Rh^{3+} significantly increased photoactivity in the liquid-phase photodegradation of $CHCl_3$, while Co^{3+} and Al^{3+} doping decreased the photoactivity [7]. Nagaveni et al. developed W, V, Ce, Zr, Fe and Cu ion-doped anatase TiO_2 nanoparticles by a solution combustion method and found that the solid formation was limited to a narrow range of concentrations of the dopants ions [16]. Kisch et al. reported Pt^{4+} doped TiO_2 exhibited higher visible photoactivity on the degradation of 4-chlorophenol [18]. Among these transition metal elements, Fe^{3+} was considered as an interesting dopant of TiO_2 and most of the investigations have been carried out by preparation of Fe-doped TiO_2 using chemical and physical methods [19–28]. It was believed that Fe doping procedure directly influences the intrinsic properties of TiO_2, such as charge carried recombination rates, the particle size and interfacial electron-transfer rates and extending photoresponse of TiO_2 into the visible range [19,21,22,27–28]. However, it was also reported that Fe^{3+} cations doping introduced an impurity level into the band gap was detrimental to the photocatalytic activity under UV light irradiation due to recombination of the generated hole and electron on the impurity level [6,7,21].

Many studies have been carried out to improve the photocatalytic activity by reducing the recombination reaction by the deposition of noble metals such as Au, Ag, Pt, Pd on the surface of TiO_2 and it was confirmed that the deposition of noble metal on TiO_2 nanoparticles was an essential factor for maximizing the

efficiency of photocatalytic reactions [29–35]. The noble metal which acts as a sink for photo-induced charge carriers, promotes interfacial charge-transfer processes. Additionally, recent investigations on gold titania nanocomposite particles also show that the presence of nanosized gold particles supported on TiO_2 extended the response of the photocatalyst into visible light region by the surface plasmon absorption of the gold [36,37]. It is now well established that the catalytic properties of Au depends on the support, the preparation method and particularly the shape and size of the Au clusters [38–44]. However, these studies were primarily concerned with Au deposition on the undoped TiO_2 or P25 titania for photocatalytic application. There have been few research focusing on Au deposition on the surface of modified TiO_2 [45–47]. Therefore, enlightened by the respective advantages of transition metal doping and deposition of noble metal, we deposited Au nanoparticles on the modified TiO_2 (Fe doped TiO_2) aiming to develop a novel photocatalyst with good performance under both visible light and UV light irradiation. Moreover, to study of gold deposited over modified TiO_2 for photocatalytic application is also an interesting topic. We previously reported Fe-doped TiO_2 prepared by the combination of sol–gel process with hydrothermal treatment and this Fe-doped TiO_2 photocatalyst exhibited visible activity during the degradation of methyl orange. The effect of Fe^{3+} dopant has been studied in our group [27]. Zanella et al. reported a promising way to prepare Au/TiO_2 by deposition–precipitation with urea for CO oxidation, by which can reach a high Au loading and small Au particle size [48]. Herein, we have developed a novel TiO_2 photocatalyst by Fe^{3+} doping together with Au deposition (using deposition–precipitation with urea) and its photocatalytic activity has been tested for degradation of organic compound under both UV light and visible light irradiation. As expected, the Au/Fe–TiO_2 photocatalyst with excellent visible light and UV light activity has been demonstrated and Fe^{3+} and Au had synergistic effects on improving the photocatalytic activity under both visible and UV light irradiation. To the best of our knowledge, such researches concerning this field have never been reported.

2. Experimental

2.1. Catalyst preparation

The preparation procedure of Fe^{3+} doped TiO_2 deposited with Au consists of two steps. Firstly, the Fe^{3+} doped TiO_2 was prepared by combining sol-gel method with hydrothermal treatment. 6 mL tetrabutyl titanate was dissolved into 34 mL anhydrous ethanol (solution A), solution B consisted of 17 mL anhydrous ethanol, 0.4 mL nitric acid, 1.6 mL distilled water and $Fe(NO_3)_3$ in the required stoichiometry (Fe/Ti = 0.57%, molar ratio). Then solution A was added drop-wise to solution B under stirring magnetically. The resultant mixture was stirred at room temperature for 2 h to hydrolysis until the transparent sol was obtained. The sol was then aged for 2 days until the formation of gel, which was then transferred into a 100-mL Teflon-inner-liner stainless steel autoclave. The autoclave was kept for 10 h under 453 K for crystallization. After this hydrothermal treatment, the precipitate was washed, dried and ground to obtain Fe^{3+} doped TiO_2 nanoparticles. Undoped TiO_2 was also prepared by the same way without adding $Fe(NO_3)_3$. Secondly, One gram of Fe–TiO_2 was added to 100 mL of amount aqueous solution containing $HAuCl_4$ (2.4×10^{-2} M) and urea (0.42 M). The suspension thermostated at 353 K was vigorously stirred for 4 h. Decomposition of urea leads to a gradual rise in pH. These sequences of preparation in solution were performed in the dark, since light is known to decompose the gold precursors and to reduce them. The solids gathered after

centrifugation were washed with deionized water four times, and then dried under vacuum at 373 K for 2 h in the dark, calcined at 673 K under a flow of industrial air (100 ml min^{-1}) with a heating rate of 2 K min^{-1} and then maintained 4 h.

Au weight loading of the sample is expressed in grams of Au per grams of sample: wt%Au = $[m_{Au}/(m_{Au} + m_{Fe-TiO2})] \times 100$. The nominal content of Au in the samples was 0.0, 2.0, 3.0 wt%, designated as 0.57Fe-TiO_2, 2.0Au/0.57Fe-TiO_2, 3.0Au/0.57Fe–TiO_2, respectively. Undoped TiO_2 deposited with 2.0, 3.0 wt% Au are designated as 2.0Au/TiO_2, 3.0Au/TiO_2, respectively. All chemicals are of analytical grade and used without further purification.

2.2. Catalyst characterization

X-ray diffraction (XRD) analysis of the prepared photocatalysts was carried out at room temperature with a Rigaku D/max 2550 VB/PC apparatus using Cu Kα radiation (λ = 1.5406 Å) and a graphite monochromator, operated at 40 kV and 30 mA. Diffraction patterns were recorded in the angular range of 10°–80° with a stepwidth of $0.02° s^{-1}$. The surface morphologies and particle sizes were observed by high-resolution transmission electron microscopy (HRTEM, JEM-2011), using an accelerating voltage of 200 kV. The S_{BET} of the samples were determined through nitrogen physical adsorption at 77 K (Micromeritics ASAP 2010). All the samples were degassed at 473 K before the measurement. The actual content of Au deposited on TiO_2 and 0.57Fe–TiO_2 was determined by atomic absorption flame emission spectroscopy (Shimadzu AA-6400F). Raman measurements were performed at room temperature using a Via+ Reflex Raman spectrometer with the excitation light of 514 nm. To analyze the light absorption of the photocatalysts, UV–vis diffuse reflectance spectra (DRS) were obtained using a scan UV–vis spectrophotometer (Varian Cary 500) equipped with an integrating sphere assembly, while $BaSO_4$ was used as a reference. To investigate the chemical states of the photocatalysts, X-ray photoelectron spectroscopy (XPS) was recorded with PerkinElmer PHI 5000C ESCA Systerm with Al Kα radiation operated at 250 W. The shift of binding energy due to relative surface charging was corrected using the C 1s level at 284.6 eV as an internal standard. The recombination of electron–hole in the samples was studied by the photoluminescence (PL) emission spectra, which was measured on a luminescence spectrometry (Cary Eclips) at room temperature under the excitation light at 280 nm. The conditions are fixed as far as possible in order to compare the photoluminescence intensity directly.

2.3. Photocatalytic activity test

The photocatalytic activity of each sample was evaluated in terms of the degradation of 2,4-dichlorophenol (2,4-DCP). 2,4-dichlorophenol (2,4-DCP) was chosen as a model pollutant to evaluate the photocatalytic activities. The photocatalyst (0.08 g) was added into an 100-mL quartz photoreactor containing 80 mL of a 50-mg L^{-1} 2,4-DCP solution. The mixture was sonicated for 10 min and stirred for 30 min in the dark in order to reach the adsorption–desorption equilibrium. A 1000-W tungsten halogen lamp equipped with a UV cut-off filters (λ > 420 nm) was used as a visible light source (the average light intensity was 60 mW cm^{-2}) and a 300-W high-pressure Hg lamp for which the strongest emission wavelength is 365 nm was used as a UV light source (the average light intensity was about 1230 μW cm^2). The lamp was cooled with flowing water in a quartz cylindrical jacket around the lamp, and ambient temperature is maintained during the photocatalytic reaction. At the given time intervals, the analytical samples were taken from the mixture and immediately centrifuged, then filtered through a 0.22-μm Millipore filter to remove the photocatalysts. The concentration of the filtrate was analyzed

by checking the absorbance at 284 nm with a UV–vis spectro-photometer (Varian Cary 100).

The reproducibility was checked by repeating the measurements at least three times and was found to be within the acceptable limit (±5%).

3. Results and discussion

3.1. Characterization

3.1.1. X-ray diffraction

The XRD patterns of the samples are shown in Fig. 1. It can be seen that the diffraction peaks of all samples are ascribed to the peaks of TiO$_2$ anatase phase [JCPDS no.21-1272, spacegroup: I4$_1$/amd (1 4 1)]. No significant characteristic peak of iron oxide can be found in Fe-doped TiO$_2$, due to lower amount of iron. Furthermore, no distinct peaks corresponding to Au phase was observed in the case of the samples containing Au, indicating of smaller crystallite size of Au or Au particles well dispersed on the surface of TiO$_2$ and Fe-doped TiO$_2$.

The average crystallizes size of all the samples are estimated using the Scherrer equation:

$$D = \frac{K\lambda}{\beta \cos\theta}$$

where β is the half-height width of the diffraction peak of anatase, $K = 0.89$ is a coefficient, θ is the diffraction angle, and λ is the X-ray wavelength corresponding to the Cu Kα radiation. The crystallite size of all samples calculated for anatase (1 0 1) peak is shown in Table 1. As can be seen from Table 1, the crystallite sizes of Fe-doped TiO$_2$ is slightly lower than that of non-doped TiO$_2$, indicating the occurrence of a slight lattice distortion in the anatase structure. The dimension decrease is caused by a number of defects in the anatase crystallites produced by the substitution of part of the Ti^{4+} site by Fe^{3+} ions, which may hinder crystallite growth [26]. Additionally, with respect to the Au/TiO$_2$ samples and Au/0.57 Fe–TiO$_2$ samples, no obvious changes on their crystallite size is observed after Au deposited on the non-doped TiO$_2$ or Fe-doped TiO$_2$. Therefore, it can be concluded that Au deposited on the surface of TiO$_2$ lead to less impact on the crystalline phase, crystalline size, and crystallinity of TiO$_2$.

3.1.2. BET-specific surface areas

As is shown from Table 1, all samples have large surface areas, which may contribute to the high photocatalytic activities of the

Table 1
The crystal sizes and BET surface area and weight percentage of Au of different samples.

Sample	Particle size (nm)[a]	S_{BET} (m^2/g)	Au content (wt%)[b]
TiO$_2$	10	153	–
0.57Fe–TiO$_2$	9	158	–
2.0Au/TiO$_2$	10	143	1.3
3.0Au/TiO$_2$	10	154	2.9
2.0Au/0.57Fe–TiO$_2$	9	148	1.8
3.0Au/0.57Fe–TiO$_2$	9	153	2.7

[a] Determined by XRD using Scherrer equation.
[b] Determined by atomic absorption flame emission spectroscopy.

samples. All of samples have similar value of the particle sizes and specific surface areas, such similarities in physicochemical properties make it convenient to study the effects of Fe^{3+} and Au on the performance of these photocatalysts.

3.1.3. Atomic absorption flame emission spectroscopy (AAS) studies

The actual content of Au in different samples is determined by AAS, the results are also listed in Table 1. It is shown that the actual content of Au measured by AAS is close to the theoretical value, indicating that most of Au in solution is deposited on the surface of TiO$_2$ or Fe–TiO$_2$ by deposition–precipitation with urea. This result is consistent with the literature reported [48].

3.1.4. Transmission electron microscopy (TEM)

TEM images of 3.0Au/0.57Fe–TiO$_2$ and 3.0Au/TiO$_2$ are shown in Fig. 2. The micrographs of these catalysts (b and d) show that the gold particles are highly dispersed on the surface of non-doped TiO$_2$ and Fe doped TiO$_2$, and the mean diameter of gold particles estimated from the TEM images are 9 nm for the non-doped TiO$_2$ samples and 8 nm for the Fe-doped TiO$_2$ samples. Compared with 3.0Au/TiO$_2$, the lower Au particle size of 3.0Au/Fe–TiO$_2$ may result by the presence of defects between the anatase crystallite produced by the substitution of part of the Ti^{4+} site by Fe^{3+} ions, which could work as particle pinning centers of the gold particles for hindering their diffusion as well as preventing the formation of larger gold particles. This result is in good agreement with literature proposals [49]. It also can be shown that the matrix TiO$_2$ and Fe-doped TiO$_2$ have the mean particle size of 10 nm and 9 nm, respectively, which is in consistent with the result of XRD. Fig. 2a and c showed that gold particles are highly crystallized and well dispersed.

3.1.5. Raman studies

Raman spectra of the samples are shown in Fig. 3. The Raman spectra of all the samples are characterized by a strong band at 144 cm^{-1}, three middle intensity bands at 394 cm^{-1}, 514 cm^{-1}, 638 cm^{-1}, and a weak band at 197 cm^{-1}. These peaks can be assigned to the fundamental vibration modes of anatase TiO$_2$ with the symmetries of E$_g$, B$_{1g}$, A$_{1g}$, E$_g$ and E$_g$ [50,51], respectively, and these results are consistent with the XRD measurements. No Raman lines due to iron oxide can be observed in the Fe^{3+} doped samples, confirming Fe^{3+} may present in the substitutional positions in the lattice of TiO$_2$.

3.1.6. UV–vis diffuse reflectance spectra

The UV–vis diffuse reflectance spectra of samples are presented in Fig. 4. The spectrum of 0.57Fe–TiO$_2$ shows a significant enhancement of light absorption at a wavelength of 400–600 nm compared with non-doped TiO$_2$. The origin of this visible light absorption is due to the formation of a dopant energy level within the band gap of TiO$_2$. The excitation of 3d electrons of Fe^{3+} transferring from the dopant energy level to the conduction band
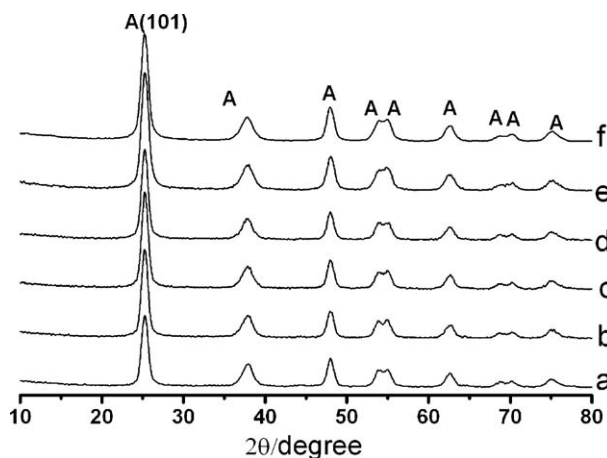

Fig. 1. XRD patterns of different samples: (a) TiO$_2$, (b) 0.57Fe–TiO$_2$, (c) 2.0Au/0.57Fe–TiO$_2$, (d) 2.0Au/TiO$_2$, (e) 3.0Au/0.57Fe–TiO$_2$, (f) 3.0Au/TiO$_2$.
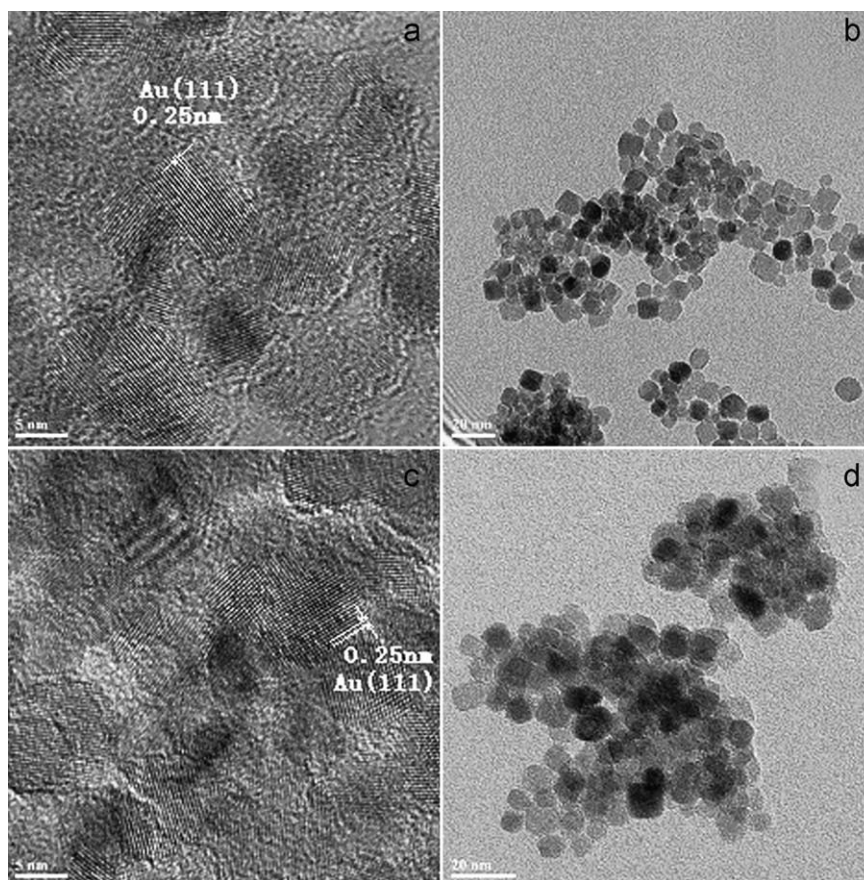
Fig. 2. TEM micrographs of the different samples: (a and b) 3.0Au/0.57Fe–TiO$_2$; (c and d) 3.0Au/TiO$_2$.

of TiO$_2$ could effectively shift the band edge absorption threshold to visible light region [6]. 2.0Au/0.57Fe–TiO$_2$ and 2.0Au/TiO$_2$ show a strong absorption peak at 500–600 nm due to the plasmon resonance of Au, which arises from the collective oscillations of the free conduction band electrons that are induced by the incident electromagnetic radiation [34,52]. The absorption of 2.0Au/TiO$_2$ and 2.0Au/0.57Fe–TiO$_2$ centered at 537 nm, 563 nm, respectively. That indicates that the surface of plasmon band of 2.0Au/0.57Fe–TiO$_2$ shifts toward longer wavelength. According to the literature proposal [34], for Au/TiO$_2$ samples, the surface plasmon resonance of metallic nanoparticles is sensitive to the particle size, shape,

load and surrounding environment. So the shift of plasmon band of 2.0Au/0.57Fe–TiO$_2$ would be attributed to its different surrounding environment of Au particles from that of 2.0Au/TiO$_2$ and there may existence of interactions between Au particles and Fe–TiO$_2$.

3.1.7. XPS spectra

The XPS spectra of the samples are shown in Fig. 5. With respect to the XPS peaks of Ti 2p, although there are slight differences in the locations of binding energies of Ti 2p$_{1/2}$ and Ti 2p$_{3/2}$ among different samples, they are all still in good agreement with the values of Ti^{4+}. No broad FWHM (full width half maximum) of Ti 2p$_{3/2}$ signals also indicate the only presence of Ti^{4+} species [53].
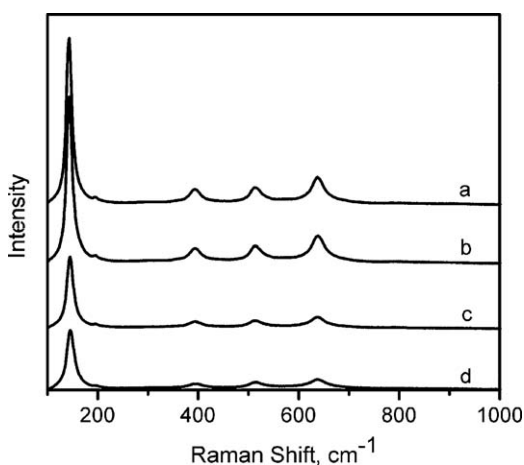

Fig. 3. Raman spectra of (a) TiO$_2$, (b) 0.57Fe–TiO$_2$, (c) 2.0Au/TiO$_2$, (d) 2.0Au/0.57Fe–TiO$_2$.
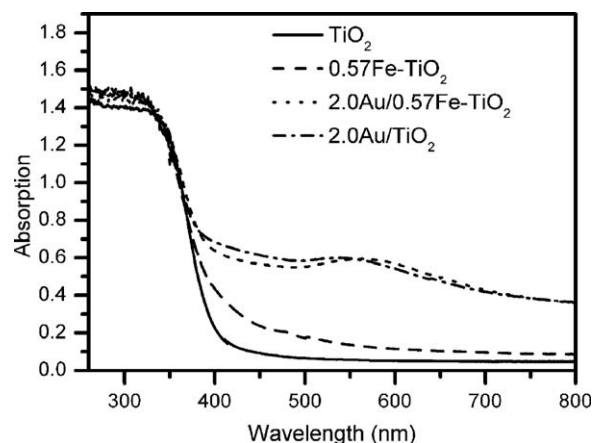

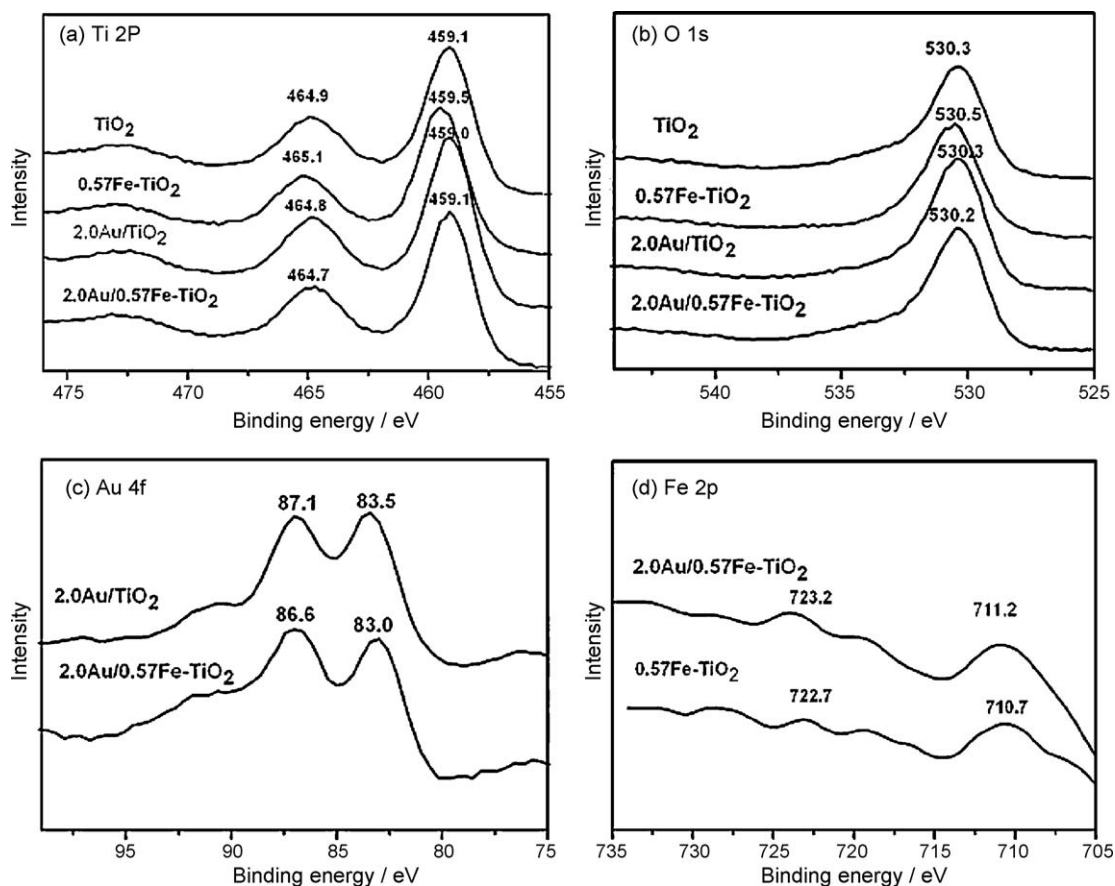**Fig. 4.** UV–vis diffuse reflectance spectra of various samples.

Fig. 5. XPS spectra of various samples: (a) Ti 2p, (b) O 1s, (c) Au 4f, (d) Fe 2p.

The O 1s binding energies of all the samples are located at a little higher value than 530.0 eV, which is assigned to bulk oxide (O^{2-}) in the TiO_2 lattice. Therefore, it can be concluded that no obvious changes on the chemical state of Ti and O can be caused by doped Fe^{3+} and deposited Au. The Au $4f_{7/2}$ and Au $4f_{5/2}$ binding energies at 83.5 eV, 87.1 eV for $2.0Au/TiO_2$ and at 83.0 eV, 86.6 eV for the $2.0Au/0.57Fe–TiO_2$ are identical to the values of fully reduced Au reported by other groups, which suggesting Au species exist in their metallic state [54,55]. Zanella et al. [56] reported oxidation gold can be completely reduced in metallic gold when the Au/TiO_2 catalyst prepared by deposition–precipitation with urea was calcinated at temperature above 473 K under air flow. Although the signals indicate that Au exists as Au^0 in $2.0Au/0.57Fe–TiO_2$ and $2.0Au/TiO_2$, the Au 4f binding energies of the former are negative shift (0.5 eV), indicating some charges may be transferred to Au species on the surface of TiO_2. The Fe 2p XPS spectra show extremely low contents of Fe on the surface of $0.57Fe–TiO_2$ and $2.0Au/0.57Fe–TiO_2$. Binding energy of Fe $2p_{3/2}$ and Fe$2p_{1/2}$ at 710.7 eV, 722.7 eV for $0.57Fe–TiO_2$ sample and at 711.2 eV, 723.2 eV for $2.0Au/0.57Fe–TiO_2$ sample suggest that Fe species are present in the oxide state [27]. Compared with $0.57Fe–TiO_2$, the positive shift of Fe 2p (0.5 eV) for $2.0Au/0.57Fe–TiO_2$ indicates charges of Fe may transfer to Au species. It can be concluded that there may exist strong interactions between Au and Fe–TiO_2, which may change the electronic property of $Au/0.57Fe–TiO_2$. This result is in consistent with conclusion by the shift of plasmon band of $2.0Au/0.57Fe–TiO_2$.

3.1.8. PL measurement

Photoluminescence (PL) emission is useful to disclose the efficiency of charge carrier trapping, immigration and transfer, and to understand the fate electron–hole pairs in semiconductor particles [19]. In this study, the PL emission spectra of several samples were examined in the wavelength range of 320–500 nm, as shown in Fig. 6. It can be observed that the positions of the peaks around 380 nm which is assign to emission of the band gap transition [57,58] are similar while PL intensities are different among these samples. The PL intensity of $0.57Fe–TiO_2$ is the highest among all samples, indicating the recombination of electron and hole has been promoted in $0.57Fe–TiO_2$. It may be explained as that Fe^{3+} act as recombination center for the photogenerated charge carriers. $2.0Au/TiO_2$ and $2.0Au/0.57Fe–$
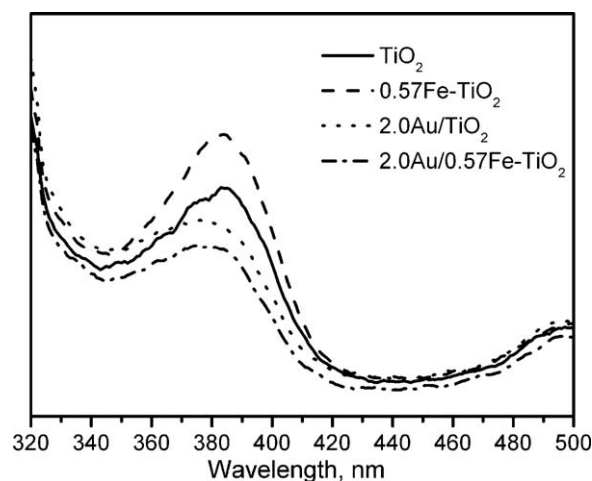

Fig. 6. Photoluminescence spectra of various samples.

TiO_2 exhibit a significantly declined PL intensity compared with TiO_2, demonstrating electron–hole recombination has been suppressed in these two samples [37]. This may due to the presence of Au on the surface of TiO_2 favor the migration of photo-produced electron to gold, thus improving the electron–hole separation. Although Fe^{3+} favors electron–hole recombination in 0.57Fe–TiO_2, this effect can be greatly weakened by Au deposited on 0.57Fe–TiO_2 because photo-produced electrons are rapidly trapped by Au and the remaining holes are trapped by Fe^{3+}, the recombination rate of electron–hole pair decreases, so the intensity is the lowest in 2.0Au/0.57Fe–TiO_2. The decrease of PL intensity can benefit enhancement of photocatalytic activity of the samples [59,60].

3.2. Photocatalytic activity

We have reported TiO_2 photocatalysts by Fe^{3+} doping together with Au deposition for the degradation of methyl orange (MO) under UV light and visible light and found that the optimum Au dosage is 3.0 wt% under UV light irradiation and 2.0 wt% under visible light irradiation [61]. However, some researchers thought the dye, not TiO_2 was excited by visible light in the presence of TiO_2 and injected an electron into the conduction band of TiO_2, from where it was scavenged by preadsorbed oxygen to form active radicals [62]. That is to say that the sensitization of dye leads to the photoreactivity of TiO_2 in the visible light region. In order to eliminate the sensitization of dye, 2,4-dichlorophenol (2,4-DCP) solutions owing to its colorless and no absorption in the visible region were selected to be the target pollutants which are degraded under UV light and visible light illumination. Fig. 7 shows that the degradation rate of 2,4-DCP under visible light in the presence of TiO_2, 0.57Fe–TiO_2, 2.0Au/TiO_2 and 2.0Au/0.57Fe–TiO_2. Under visible light, undoped TiO_2 exhibits almost no activity, 10% loss of 2,4-DCP may result by polymerization of 2,4-DCP [63]. Fe doped TiO_2 sample shows good photocatalytic activity. Since Fe^{3+} ions can enhance the intensity of absorption in the visible light region and make a red shift in the band gap transition of the Fe-doped TiO_2 samples. This can induce more photo-generated electrons and holes to participate in the photocatalytic reactions. Apart from this effect, Fe^{3+} ions can also serve as a mediator of the transfer of interfacial charge at an appropriate doping concentration [27]. In addition, 2.0Au/TiO_2 also has better performance than undoped TiO_2, because Au particles deposition can not only extend the response to visible light region due to the plasmon resonance of Au, but also capture electrons, resulting in the inhibition of electron–hole recombination. Clearly, 2.0Au/0.57Fe–TiO_2 exhibits

the highest photocatalytic activity for the degradation of 2,4-DCP, besides including advantages of Fe doping and Au deposition, this also may be owing to the synergistic effects of doped Fe^{3+} and deposited Au on the enhancement of visible light activity. That can be explained as follow: Fe^{3+} presents in the substitution positions in the TiO_2 lattice would introduce a dopant energy level into the band gap of TiO_2 as well as the plasmon resonance of Au particles result in absorption into the visible region [19,34]. Under visible light illumination, the electrons can be excited from the dopant level to the conduction band [7,19], then they are transferred to Au^0 deposited on the surface of TiO_2, which can enhance the electron–hole separation and the subsequent transfer of the trapped electrons to the adsorbed O_2 molecules [54]. Thus the photocatalytic activity can be efficiently improved.

The photodegradation of 2,4-DCP under UV light in the presence of TiO_2, 0.57Fe–TiO_2, 3.0Au/TiO_2, 3.0Au/0.57Fe–TiO_2 and P25 is shown in Fig. 8. It is shown that under UV light illumination, the photocatalytic activity of 0.57Fe–TiO_2 decreased compared with undoped TiO_2, which is in agreement with other groups [29]. It can be attributable to the detrimental effect of Fe^{3+} in increasing electron–hole recombination which has been confirmed by PL measurement. A lot of electrons from the valence band are excited to the conduct band under UV irradiation owing to UV light with higher energy. However, these generated electrons would be trapped by Fe^{3+} in the lattice TiO_2 rather than be transferred to the surface of TiO_2. Meanwhile, many generated holes could also be scavenged by Fe^{3+}, thus Fe^{3+} become the recombination center and result in the decrease of UV light photoactivity of Fe doped TiO_2 [29]. Additionally, 3.0Au/TiO_2 is more photoactive than TiO_2 because of the same positive role played by Au as under visible light illumination. Compared to the other three samples, 3.0Au/0.57Fe–TiO_2 exhibits higher photo-catalytic activity, even close to P25, a well-known commercial photocatalyst with high UV photoactivity. The higher photoactivity of 3.0Au/0.57Fe–TiO_2 may be attributed to the following reasons. The synergistic effects of doped Fe^{3+} and deposited Au are responsible for enhancement photocatalytic performance. Under UV light illumination, the excited electrons can be trapped by Au; meanwhile the remaining holes are trapped by Fe^{3+} and then transferred to the surface to initiate the photocatalytic processes. The mechanism of degradation of 2,4-DCP under UV light illumination is different from that of under visible light. It was reported that Au/TiO_2 photocatalysts with small Au particle size and 0.5–2% loading were more active. Orlov et al. and Tian et al. reported Au/P25 catalyst with Au particle size of 3 nm and 1% Au loading exhibited higher photocatalytic activity for the photo-
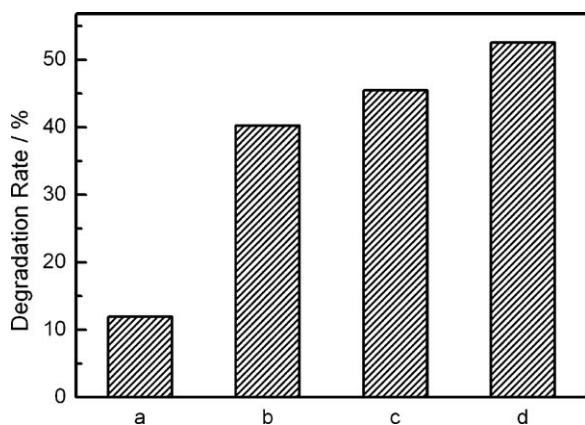

Fig. 7. Photocatalytic degradation rate of 2,4-DCP under visible light illumination for 5 h over (a) TiO_2, (b) 0.57Fe–TiO_2, (c) 2.0Au/TiO_2, (d) 2.0Au/0.57Fe–TiO_2.
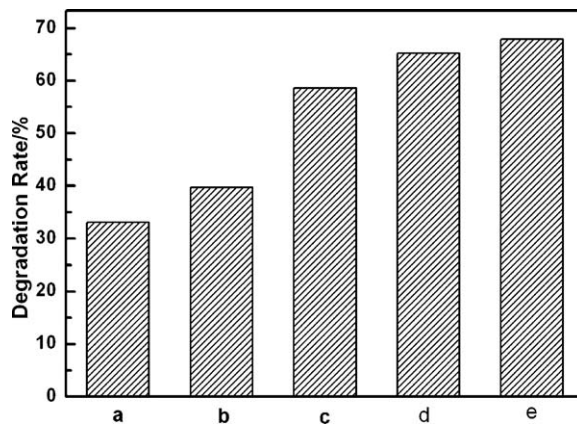

Fig. 8. Photocatalytic degradation rate of 2,4-DCP under UV light illumination for 2.5 h over (a) 0.57Fe–TiO_2, (b) TiO_2, (c) 3.0Au/TiO_2, (d) 3.0Au/0.57Fe–TiO_2, (e) P25.

catalytic degradation of methyl *tert*-butyl ether (MTBE) and methyl orange [40,42]. González et al. found Au/Al_2O_3–TiO_2 photocatalyst with Au particle size of 7 nm and 0.55% Au loading had better activity for degradation of MTBE [39]. However, the 3.0Au/0.57Fe–TiO_2 with Au particle size of 8 nm showed higher activity for degradation of 2,4-DCP. It seems that our result is inconsistent with other groups. We propose that the photocatalytic performance of Au/TiO_2 is dependent on not only Au particle size but also the properties of TiO_2. Our previous study revealed that the Au particles with an appropriate size can possess an energy level between the conduct band of TiO_2 and the adsorbed O_2. Thus, the photoelectrons can be captured by gold particles and subsequently be transferred to the adsorbed O_2, leading to the effective separation of electrons and holes, and consequently increasing the photocatalytic activity of TiO_2. While too large or too small gold particles size is disadvantage of transferring photo-electrons [42]. With regards to photocatalytic reaction, it should be note that both chemical and physical properties of TiO_2 such as particle size, phase composition, surface area and concentration of lattice defects and impurities can have great influence on its performance [64]. It is also suggested that particle size of TiO_2 is a crucial factor in the dynamics of the electron/hole recombination process, in large TiO_2 nanoparticles, bulk recombination of the charge carriers was the dominant process, which could be reduced by a decrease in particle size; as the particle size become very small, surface recombination process became dominant [65]. In the 3.0Au/0.57Fe–TiO_2 sample, the particle size of Fe-doped TiO_2 is about 9 nm, which is quite different from P25 with particle size of 30 nm. Under UV light irradiation, with respect to the 3.0Au/Fe-doped TiO_2 sample, most of the electrons and holes were generated close to the surface and surface recombination was dominant process. When Au deposited on the surface of Fe-doped TiO_2, the excited electrons close to the surface were transferred from TiO_2 to Au nanoparticles, improving the charge separation and hence inhibition of surface recombination process [66]. Thus, the effect of Au particle size on photocatalytic performance is relative to the properties of TiO_2.

In most studies, the deposition of a noble metal on semi-conductor nanoparticles is in general beneficial for maximizing the efficiency of photocatalytic reactions. However, it is suspected that the deactivation of catalyst surface in Au doped TiO_2 may be faster than undoped TiO_2. Because the generated–hole at the TiO_2 surface and hydroxyl radicals during the photocatalytic reaction may oxidize Au into Au ion [67]. This will adversely affect on the life of the photocatalyst so the increase in activity of the TiO_2 will be for short span and the catalyst cannot be used for long term.

In our case, no noticeable differences were observed in the UV–vis absorption spectra and TEM image of the 3.0Au/0.57Fe–TiO_2 photocatalysts before and after the photocatalytic reaction (not shown). This excludes the possibility of further oxidation of Au intercalation of Au^+ into TiO_2 and aggregation of Au particle during photocatalysis. Arabatzis et al. [68] and Sonawane et al. [39] have reported that no appreciable deactivation of Au/TiO_2 film was observed when Au/TiO_2 film was applied for degradation of MO under UV light and decomposition of phenol in sunlight. It is known that the oxide-containing radicals, especially hydroxyl radical, act as the active agents for the decomposition of the organic compounds. The researches on mechanism of photocata-lytic degradation of MO show that hydroxyl radicals prefer to attack the electron-rich sites of MO and result the formation intermediate organic species and subsequently complete oxidation of these species to water and carbon dioxide [69]. Therefore, we assume that hydroxyl radical seems to take precedence over the oxidation of organic compounds rather than Au species loaded on TiO_2 surface.

4. Conclusions

Fe^{3+} doped TiO_2 deposited with Au (Au/Fe–TiO_2) has been synthesized. Results of various characterization methods indicate Fe^{3+} presents in the substitutional position in the lattice of TiO_2, and Au exists as Au^0 on the surface of the samples. Photocatalytic experiments show that Fe^{3+} and Au have synergistically improved the photocatalytic activity of TiO_2 under both visible light and UV light illumination. Explanation for the synergistic effects of Fe^{3+} and Au under visible light and UV light illumination has been discussed. Under visible light illumination, Fe^{3+} plays a role in extending light absorption into the visible region, and Au acts as traps for visible light-induced electrons, resulting in reduction of recombination. Under UV light illumination, the excited electrons can be trapped by Au; meanwhile the remaining holes are trapped by Fe^{3+} and then transferred to the surface to initiate the photocatalytic processes.

References

[1] A. Fujishima, T.N. Rao, D.A. Tryk, J. Photochem. Photobiol. C 1 (2000) 1–21.
[2] E.J. Wolfrim, J. Huang, D.M. Blake, P. Maness, Z. Huang, J. Fiest, Environ. Sci. Technol. 36 (2002) 3412–3419.
[3] C. Hu, J.C. Yu, Z. Hao, P.K. Wong, Appl. Catal. B: Environ. 42 (2003) 47–55.
[4] M.R. Hoffmann, S.T. Martin, W. Choi, D.W. Bahnemann, Chem. Rev. 95 (1995) 69–96.
[5] J.C. Yu, W. Ho, J. Yu, H. Yip, P.K. Wong, J. Zhao, Environ. Sci. Technol. 39 (2005) 1175–1179.
[6] X.H. Wang, J.G. Li, H. Kamiyama, Y. Moriyoshi, T. Ishigaki, J. Phys. Chem. B 110 (2006) 6804–6809.
[7] W. Choi, A. Termin, M.R. Hoffmann, J. Phys. Chem. 98 (1994) 13669–13679.
[8] R. Asashi, T. Morikawa, T. Ohwakl, K. Aoki, Y. Taga, Science 293 (2001) 269–271.
[9] C. Burda, Y. Lou, X. Chen, A.C. Samia, J. Stout, J.L. Gole, Nano Lett. 3 (2003) 1049–1051.
[10] Y. Cong, J.L. Zhang, F. Chen, M. Anpo, D. He, J. Phys. Chem. C 111 (2007) 10618–10623.
[11] J. Kiwi, M. Graetzel, J. Phys. Chem. 90 (1986) 637–640.
[12] K.E. Karakitsou, X.E. Verykios, J. Phys. Chem. 97 (1993) 1184–1189.
[13] S.C. Martin, C.L. Morrison, M.R. Hoffmann, J. Phys. Chem. 98 (1994) 13695–13704.
[14] J.F. Zhu, F. Chen, J.L. Zhang, H.J. Chen, M. Anpo, J. Mol. Catal. A 216 (2004) 35–43.
[15] J.F. Zhu, Z.G. Deng, F. Chen, J.L. Zhang, H.J. Chen, M. Anpo, J.Z. Huang, Appl. Catal. B: Environ. 62 (2006) 329–335.
[16] K. Nagaveni, M.S. Hegde, G. Madras, J. Phys. Chem. B 108 (2004) 20204–20212.
[17] S. Klosek, D. Raftery, J. Phys. Chem. B 105 (2001) 2815–2819.
[18] H. Kisch, L. Zang, C. Lange, W.F. Maier, C. Antonius, D. Meissner, Angew. Chem. Int. Ed. 37 (1998) 3034–3036.
[19] H. Yamashita, M. Harada, J. Misaka, M. Takeuchi, B. Neppolian, M. Anpo, Catal. Today 84 (2003) 191–196.
[20] J.A. Navio, G. Colon, M.I. Litter, G.N. Bianco, J. Mol. Catal. A: Chem. 106 (1996) 267–276.
[21] Y.H. Zhang, S.G. Ebbinghaus, A. Weidenkaff, T. Kurz, K.V. Nidda, P.J. Klar, M. Guengerich, A. Reller, Chem. Mater. 15 (2003) 4028–4033.
[22] J. Soria, J.C. Conesa, V. Augugliaro, L. Palmisano, M. Schiavello, A. Sclafani, J. Phys. Chem. 95 (1991) 274–282.
[23] M.I. Litter, J.A. Navio, J. Photochem. Photobiol. A: Chem. 98 (1996) 171–181.
[24] K.T. Ranjit, B. Viswanathan, J. Photochem. Photobiol. A: Chem. 108 (1997) 79–84.
[25] E. Piera, M.I. Tejedor, M.E. Zorn, M.A. Anderson, Appl. Catal. B: Environ. 46 (2003) 671–685.
[26] J. Navio, G. Colon, M. Macias, C. Real, M. Litter, Appl. Catal. A: Gen. 177 (1999) 111–120.
[27] J.F. Zhu, F. Chen, J.L. Zhang, H.J. Chen, M. Anpo, J. Photochem. Photobiol. A: Chem. 180 (2006) 196–204.
[28] C. Adan, A. Bahamonde, M. Fernandez-Garcia, A. Martinez-Arias, Appl. Catal. B: Environ. 72 (2007) 11–17.
[29] A.D. Paola, G. Marci, L. Palmisano, M. Schiavello, K. Uosaki, S. Ikeda, B. Ohtani, J. Phys. Chem. B 106 (2002) 637–645.

[30] L. Zang, W. Macyk, C. Lange, W.F. Maier, C. Antonius, D. Meissner, H. Kisch, Chem. Eur. J. 6 (2000) 379–384.
[31] M. Bowker, D. James, P. Stone, R. Bennett, N. Perkins, L. Millard, J. Greaves, A. Dickinson, J. Catal. 217 (2003) 427–433.
[32] Y. Kohno, H. Hayashi, S. Takenaka, T. Tanaka, T. Funabiki, S. Yoshida, J. Photochem. Photobiol. A 126 (1999) 117–123.
[33] V. Iliev, D. Tomova, L. Bilyarska, A. Eliyas, L. Petrov., Appl. Catal. B: Environ. 63 (2006) 266–271.
[34] P.V. Kamat, J. Phys. Chem. B 106 (2002) 7729–7744.
[35] W. Kubo, T. Tatsuma, J. Mater. Chem. 15 (2005) 3104–3108.
[36] E.C.H. Sykes, F.J. Williams, M.S. Tikhov, R.M. Lambert, J. Phys. Chem. B 106 (2002) 5390–5394.
[37] X.Z. Li, F.B. Li, Environ. Sci. Technol. 35 (2001) 2381–2387.
[38] A. Orlov, D.A. Jefferson, N. Macleod, R.M. Lambert, Catal. Lett. 92 (2004) 41–47.
[39] R.S. Sonawane, M.K. Dongare, J. Mol. Catal. A: Chem. 243 (2006) 68–76.
[40] A. Orlov, D.A. Jefferson, M. Tikhov, R.M. Lambert, Catal. Commun. 8 (2007) 821–824.
[41] X. Wang, D.R.G. Mitchell, K. Prince, A.J. Atanacio, R.A. Caruso, Chem. Mater. 20 (2008) 3917–3926.
[42] B.Z. Tian, J.L. Zhang, T.Z. Tong, F. Chen, Appl. Catal. B: Environ. 79 (2008) 394–401.
[43] M.A. Centeno, M.C. Hidalgo, M.I. Dominguez, J.A. Navío, J.A. Odriozola, Catal. Lett. 123 (2008) 198–206.
[44] M. Mrowetzl, A. Villa, L. Prati, E. Sellil, Gold Bull. 40 (2007) 155–161.
[45] H.J. Kim, M.K. Han, S.M. Lee, D.K. Hwang, Y.G. Shul, Top. Catal. 47 (2008) 109–115.
[46] V. Rodríguez-González, R. Zanella, G. Angel, R. Gómeza, J. Mol. Catal. A: Chem. 281 (2008) 93–98.
[47] J.S. Li, D.L. Shieh, D.Y. Li, C.H. Ho, S.J. Yang, J.L. Lin, Appl. Surf. Sci. 254 (2008) 4655–4664.
[48] R. Zanella, S. Giorgio, C.R. Henry, C. Louis, J. Phys. Chem. B 106 (2002) 7634–7642.
[49] X. Bokhimi, R. Zanella, J. Phys. Chem. C 111 (2007) 2525–2532.
[50] H. Berger, H. Tang, J. Crys. Growth 130 (1993) 108–112.
[51] K. Mallick, M.J. Witcomb, M.S. Scurrell, Appl. Catal. A: Gen. 259 (2004) 163–168.
[52] Y.C. Liu, L.C. Juang, Langmuir 20 (2004) 6951–6955.
[53] B. Erdem, R.A. Hunsicker, G.W. Simmons, E.D. Sudol, V.L. Dimonie, M.S. El-Aasser, Langmuir 17 (2001) 2664–2669.
[54] J.H. Yang, J.D. Henao, M.C. Raphulu, Y.M. Wang, T. Caputo, A.J. Groszek, M.C. Kung, M.S. Scurrell, J.T. Miller, H.H. Kung, J. Phys. Chem. B. 109 (2005) 10319–10326.
[55] S. Kielbassa, M. Kinne, R.J. Behm, J. Phys. Chem. B 108 (2004) 19184–19190.
[56] R. Zanella, S. Giorgio, C.H. Shin, C.R. Henry, C. Louis, J. Catal. 222 (2004) 357–367.
[57] H. Tang, H. Berger, P. Schmid, F. Levy, Solid State Commun. 92 (1994) 267–271.
[58] F.B. Li, X.Z. Li, Chemosphere 48 (2002) 1103–1111.
[59] J.C. Yu, J.G. Yu, W.K. Ho, Z.T. Jiang, L.Z. Zhang, Chem. Mater. 14 (2002) 3808–3816.
[60] B. Gao, Y. Ma, Y. Cao, W. Yang, J. Yao, J. Phys. Chem. B 110 (2006) 14391–14397.
[61] L. Xiao, J.L. Zhang, Y. Cong, B.Z. Tian, F. Chen, M. Anpo, Catal. Lett. 111 (2006) 207–211.
[62] J.C. Zhao, C.C. Chen, W.H. Ma, Topic Catal. 35 (2005) 269–278.
[63] A.G. Agrios, K.A. Gray, E. Weitz, Langmuir 19 (2003) 1402–1409.
[64] X.B. Chen, S.S. Mao, Chem. Rev. 107 (2007) 2891–2959.
[65] Z. Zhang, C.C. Wang, R. Zakaria, J.Y. Ying, J. Phys. Chem. B 102 (1998) 10871–10878.
[66] M. Jacob, H. Levanon, P.V. Kamat, Nano Lett. 3 (2003) 353–358.
[67] V. Subramanian, E.E. Wolf, P.V.L. Lamat, Langmuir 19 (2003) 469–474.
[68] I.M. Arabatzis, T. Tergiopoulos, D. Andreeva, S. Kitova, S.G. Neophytides, P. Falaras, J. Catal. 220 (2003) 127–135.
[69] J.T. Spadaro, L. Isabelle, V. Renganathan, Environ. Sci. Technol. 28 (1994) 1389–1393.